AFRL-AFOSR-VA-TR-2016-0192

High-Reynolds Number Viscous Flow Simulations on Embedded-Boundary Cartesian Grids

Marsha Berger
NEW YORK UNIVERSITY

05/05/2016
Final Report

Air Force Research Laboratory
AF Office Of Scientific Research (AFOSR)/ RTA2
Arlington, Virginia 22203
Air Force Materiel Command

REPORT DOCUMENTATION PAGE

Form Approved
OMB No. 0704-0188

PLEASE DO NOT RETURN YOUR FORM TO THE ABOVE ORGANIZATION.

1. REPORT DATE *(DD-MM-YYYY)*	2. REPORT TYPE	3. DATES COVERED *(From - To)*
30/04/2016	Final	High-Reynolds

4. TITLE AND SUBTITLE

High-Reynolds Number Viscous Flow Simulations on Embedded-Boundary Cartesian Grids

5a. CONTRACT NUMBER

5b. GRANT NUMBER
FA9550-13-1-0052

5c. PROGRAM ELEMENT NUMBER

6. AUTHOR(S)
Marsha Berger

5d. PROJECT NUMBER

5e. TASK NUMBER

5f. WORK UNIT NUMBER

7. PERFORMING ORGANIZATION NAME(S) AND ADDRESS(ES)
New York University
Courant Institute of Mathematical Sciences
251 Mercer Street
New York,NY 10012

8. PERFORMING ORGANIZATION REPORT NUMBER

9. SPONSORING/MONITORING AGENCY NAME(S) AND ADDRESS(ES)
AFOSR
875 N RANDOLPH ST
ARLINGTON VA 22203

10. SPONSOR/MONITOR'S ACRONYM(S)
AFOSR

11. SPONSOR/MONITOR'S REPORT NUMBER(S)

12. DISTRIBUTION/AVAILABILITY STATEMENT
DISTRIBUTION A

13. SUPPLEMENTARY NOTES

14. ABSTRACT

Over the grant period, we developed a two-dimensional viscous steady- state flow solver for both laminar and turbulent flow. We developed a way to incorporate wall functions in non-body fitted grids by having each cut cell spawn a “linelet” from the wall through the cut cell centroid, into the Cartesian grid. We developed a fully conservative method for coupling the wall function to the flow on the Cartesian grid. We extended the wall function into a more general wall model that solves a two point boundary value problem on the linelets. The bvp includes more terms than is typically used in the diffusion model, which is what standard wall functions are based on. The improved wall model on the linelets allow them to go further into the boundary layer, reducing the Cartesian resolution requirements and allowing coarser near-wall Cartesian cells. This work was in collaboration with Michael Aftosmis, at NASA Ames Research Center.

15. SUBJECT TERMS

16. SECURITY CLASSIFICATION OF:			17. LIMITATION OF ABSTRACT	18. NUMBER OF PAGES	19a. NAME OF RESPONSIBLE PERSON
a. REPORT	b. ABSTRACT	c. THIS PAGE			19b. TELEPHONE NUMBER *(Include area code)*

Reset

INSTRUCTIONS FOR COMPLETING SF 298

1. REPORT DATE. Full publication date, including day, month, if available. Must cite at least the year and be Year 2000 compliant, e.g. 30-06-1998; xx-06-1998; xx-xx-1998.

2. REPORT TYPE. State the type of report, such as final, technical, interim, memorandum, master's thesis, progress, quarterly, research, special, group study, etc.

3. DATES COVERED. Indicate the time during which the work was performed and the report was written, e.g., Jun 1997 - Jun 1998; 1-10 Jun 1996; May - Nov 1998; Nov 1998.

4. TITLE. Enter title and subtitle with volume number and part number, if applicable. On classified documents, enter the title classification in parentheses.

5a. CONTRACT NUMBER. Enter all contract numbers as they appear in the report, e.g. F33615-86-C-5169.

5b. GRANT NUMBER. Enter all grant numbers as they appear in the report, e.g. AFOSR-82-1234.

5c. PROGRAM ELEMENT NUMBER. Enter all program element numbers as they appear in the report, e.g. 61101A.

5d. PROJECT NUMBER. Enter all project numbers as they appear in the report, e.g. 1F665702D1257; ILIR.

5e. TASK NUMBER. Enter all task numbers as they appear in the report, e.g. 05; RF0330201; T4112.

5f. WORK UNIT NUMBER. Enter all work unit numbers as they appear in the report, e.g. 001; AFAPL30480105.

6. AUTHOR(S). Enter name(s) of person(s) responsible for writing the report, performing the research, or credited with the content of the report. The form of entry is the last name, first name, middle initial, and additional qualifiers separated by commas, e.g. Smith, Richard, J, Jr.

7. PERFORMING ORGANIZATION NAME(S) AND ADDRESS(ES). Self-explanatory.

8. PERFORMING ORGANIZATION REPORT NUMBER. Enter all unique alphanumeric report numbers assigned by the performing organization, e.g. BRL-1234; AFWL-TR-85-4017-Vol-21-PT-2.

9. SPONSORING/MONITORING AGENCY NAME(S) AND ADDRESS(ES). Enter the name and address of the organization(s) financially responsible for and monitoring the work.

10. SPONSOR/MONITOR'S ACRONYM(S). Enter, if available, e.g. BRL, ARDEC, NADC.

11. SPONSOR/MONITOR'S REPORT NUMBER(S). Enter report number as assigned by the sponsoring/ monitoring agency, if available, e.g. BRL-TR-829; -215.

12. DISTRIBUTION/AVAILABILITY STATEMENT. Use agency-mandated availability statements to indicate the public availability or distribution limitations of the report. If additional limitations/ restrictions or special markings are indicated, follow agency authorization procedures, e.g. RD/FRD, PROPIN, ITAR, etc. Include copyright information.

13. SUPPLEMENTARY NOTES. Enter information not included elsewhere such as: prepared in cooperation with; translation of; report supersedes; old edition number, etc.

14. ABSTRACT. A brief (approximately 200 words) factual summary of the most significant information.

15. SUBJECT TERMS. Key words or phrases identifying major concepts in the report.

16. SECURITY CLASSIFICATION. Enter security classification in accordance with security classification regulations, e.g. U, C, S, etc. If this form contains classified information, stamp classification level on the top and bottom of this page.

17. LIMITATION OF ABSTRACT. This block must be completed to assign a distribution limitation to the abstract. Enter UU (Unclassified Unlimited) or SAR (Same as Report). An entry in this block is necessary if the abstract is to be limited.

Final Report: High-Reynolds Number Viscous Flow Simulations on Embedded-Boundary Cartesian Grids

Marsha J. Berger
Courant Institute
April, 2016

Executive Summary

The long-term goal of this research is to develop algorithms to simulate high Reynolds number turbulent flow in complicated geometries using embedded boundary grids. The main stumbling block is the lack of an affordable refinement strategy that is commonplace in structured grids - namely, the use of highly refined, high aspect ratio cells in the boundary layer. Over the grant period, we developed a two-dimensional viscous steady-state flow solver for both laminar and turbulent flow. We developed a way to incorporate wall functions in non-body fitted grids by having each cut cell spawn a "linelet" from the wall through the cut cell centroid, into the Cartesian grid. We developed a fully conservative method for coupling the wall function to the flow on the Cartesian grid. We extended the wall function into a more general wall model that solves a two point boundary value problem on the linelets. The bvp includes more terms than is typically used in the diffusion model, which is what standard wall functions are based on. The improved wall model on the linelets allow them to go further into the boundary layer, reducing the Cartesian resolution requirements and allowing coarser near-wall Cartesian cells. This work was in collaboration with Michael Aftosmis, at NASA Ames Research Center.

Research During Grant Period

In previous work during the last grant period we developed Navier Stokes solvers for laminar and viscous flows in two dimensions. In integral form the two dimensional Reynolds-averaged Navier Stokes equations are:

$$\frac{d}{dt}\iint_\Omega U\,dA + \oint_{\partial\Omega}(F\hat{i} + G\hat{j})\cdot\hat{n}\,dS = \oint_{\partial\Omega}(F_v\hat{i} + G_v\hat{j})\cdot\hat{n}\,dS \tag{1}$$

where $U = (\rho, \rho u, \rho v, \rho E)^T$, and

$$F = \begin{pmatrix} \rho u \\ \rho u^2 + p \\ \rho uv \\ u(\rho E + p) \end{pmatrix} G = \begin{pmatrix} \rho v \\ \rho uv \\ \rho v^2 + p \\ v(\rho E + p) \end{pmatrix} F_v = \begin{pmatrix} 0 \\ \tau_{xx} \\ \tau_{xy} \\ u\tau_{xx} + v\tau_{xy} - q_x \end{pmatrix} G_v = \begin{pmatrix} 0 \\ \tau_{yx} \\ \tau_{yy} \\ u\tau_{xy} + v\tau_{yy} - q_y \end{pmatrix}.$$

The Prandtl number is given by $Pr = \mu c_p/k$, and μ is computed using Sutherland's law [8]. We take $Pr = .72$. The shear stresses are

$$\begin{aligned} \tau_{xx} &= \frac{2}{3}(\mu + \mu_t)(2u_x - v_y) \\ \tau_{xy} &= (\mu + \mu_t)(u_y + v_x) \;=\; \tau_{yx} \\ \tau_{yy} &= \frac{2}{3}(\mu + \mu_t)(2v_y - u_x) \end{aligned} \tag{2}$$

and turbulent heat flux $\nabla q = (\frac{\mu c_p}{Pr} + \frac{\mu_t c_p}{Pr_t})\nabla T$.

For laminar flow, we compared several stencils for use at cut cells, found two with roughly equivalent accuracy, and implemented the one that fit better in Cart3D's finite volume infrastructure. To be able to compute skin friction, which needs $\partial u/\partial y$ at the wall, we used a quadratic in the normal direction in the cut cells, instead of the linear reconstruction used in the rest of the mesh.

For turbulent flow, we used the RANS equations and the Spalart-Allmaras (SA) turbulence model. The SA turbulence model defines the $\mu_t = \rho\nu_t$, the turbulent viscosity in Eq.(2):

$$\begin{aligned} \frac{\partial}{\partial t}(\tilde{\nu}) + \frac{\partial}{\partial x_j}(u_j\tilde{\nu}) = \frac{1}{\sigma}\left[(1 + c_{b2})\Big(\frac{\partial\tilde{\nu}}{\partial x_j}\Big)^2 + (\nu + \tilde{\nu}f(\chi))\frac{\partial^2\tilde{\nu}}{\partial x_j^2}\right] \\ +\ \text{Production}\ -\ \text{Destruction} \end{aligned} \tag{3}$$

Standard forms for these terms are

$$f(\chi) = \begin{cases} 1 & \chi > 0 \\ 1 + \frac{\chi}{2} & \text{otherwise} \end{cases}, \qquad \text{Production} = \begin{cases} c_{b1}\,\hat{S}\,\tilde{\nu} & \chi > 0 \\ c_{b1}\,\Omega\,g_n\,\tilde{\nu} & \text{otherwise} \end{cases}, \tag{4}$$

with

$$\hat{S} = \begin{cases} \Omega + \bar{S} & \bar{S} > -c_{v2}\,\omega \\ \Omega + \frac{\Omega\,(c_{v2}^2 + c_{v3}\bar{S})}{(\Omega\,(c_{v3} - 2c_{v2}) - \bar{S})} & \text{otherwise} \end{cases} \tag{5}$$

and $\bar{S} = \frac{\tilde{\nu} f_{v2}}{K^2 d^2}$, where Ω is the magnitude of vorticity. For the destruction term we have

$$\text{Destruction} = \begin{cases} c_{w1}\,f_w(\frac{\tilde{\nu}}{d})^2 & \chi \geq 0 \\ -c_{w1}\,(\frac{\tilde{\nu}}{d})^2 & \text{otherwise} \end{cases} \tag{6}$$

with $\nu_t = \tilde{\nu} f_{v1}$ and the usual definitions of f_w, g, r, χ, and the other constants[13]. We assume the flow is fully turbulent and do not include transition terms.

We developed a somewhat modified "negative" model to handle the strong transient behavior on coarse grids using multigrid. (*Negative* refers to how to handle the non-physical negative viscosity; at convergence when viscosity is back to being positive the equations are the same). Many researchers use a first order finite volume scheme to compute $\tilde{\nu}$ in (3) above, to help keep the viscosity positive. We found it necessary to use a second order method for $\tilde{\nu}$, since on non-flow-aligned grids this was simply too diffusive.

We developed a hierarchy of wall models that improve on the wall function, allowing us to use coarser background grids. The previous research period, where we developed the "quadratic" wall model used for laminar flow, and the viscous stencil used in the highly irregular cut cells, has previously been reported, and is already in the literature [2]. In this research period we developed a wall function and wall model approach, summarized below.

Analytic Wall Functions for Embedded Boundary Grids

For RANS simulations, the near-wall flow is governed by viscous stresses, as opposed to the outer flow where inertial forces dominate. This is the basis for the use of wall functions, which have been receiving renewed interest for both body-fitted [6, 12, 9, 11] and non-body-fitted immersed boundary grids [4, 7]. By looking at the asymptotics of the RANS equations, keeping the largest terms, and assuming for simplicity there is no pressure gradient, the so-called "diffusion model" can be derived,

$$\frac{\partial}{\partial y}\left((\mu + \mu_t)\frac{\partial u}{\partial y}\right) = 0 \tag{7}$$

In boundary layer ("plus") coordinates and after integrating once this becomes

$$(1 + \nu_t^+)\frac{dU^+}{dy^+} = 1 \tag{8}$$

where

$$\nu_t^+ = \nu_t/\nu, \quad U^+ = U/u_\tau, \quad \text{and} \quad y^+ = y u_\tau/\nu. \tag{9}$$

There are two regimes, $v_t^+ \ll 1$, which gives the linear behavior $U^+ = y^+$ in the viscous sublayer, and $v_t^+ \gg 1$, which gives the logarithmic layer $U^+ = (1/\kappa)\log(y^+) + B$, with $\kappa = .41$, when the turbulent viscosity is approximated using $v_t^+ = \kappa y^+$. The constant $B = 5.0333$. Spalding's wall function, given by

$$y^+(u^+) = u^+ + e^{-\kappa B}\left(e^{\kappa u^+} - 1 - \kappa u^+ - \frac{1}{2}(\kappa u^+)^2 - \frac{1}{6}(\kappa u^+)^3\right) \tag{10}$$

is a functional fit to these two regimes.

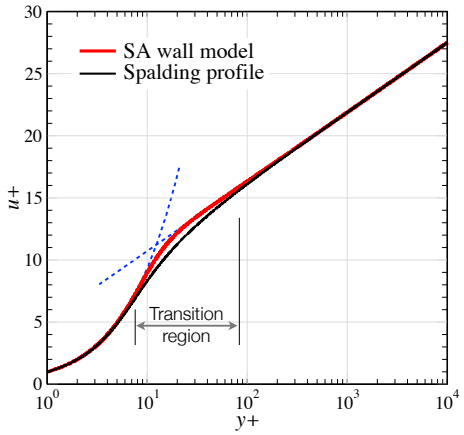

Figure 1: Comparison of SA wall model with Spalding's formula. The largest difference is in the transition region.

Recently there is a new wall function, developed by Allmaras [2, 1], which is more complicated to derive but more compatible with the limiting form of the Spalart-Allmaras model used in our RANS simulations, see Fig. 1. In final form it is

$$\begin{aligned} u^+(y^+) \;=\; \bar{B} \;+\; c_1 \log((y^+ + a_1)^2 + b_1^2) \;-\; c_2 \log((y^+ + a_2)^2 + b_2^2) \\ -\; c_3 \mathrm{ArcTan}(y^+ + a_1, b_1) \;-\; c_4 \mathrm{ArcTan}(\mathrm{y}^+ + \mathrm{a}_2, \mathrm{b}_2), \end{aligned} \tag{11}$$

where we omit the values for the many constants. Equation (11) (henceforth called the SA wall model) has the advantage over Spalding's formula of matching the profiles actually computed in the flow field by the Spalart-Allmaras turbulence model. In particular the profiles are a better match through the transition region, where the two formulas differ the most. This is evident in Fig. 1. In this figure, Spalding's formula was evaluated using $B = 5.033$ in (10) to match the asymptotic behavior of the SA model, which produces this value for the constant shift. Furthermore, (11) is more computationally efficient since given y^+, the value u^+ is explicitly evaluated rather than needing a nonlinear iteration as (10) does.[1]

The wall function is coupled to the underlying Cartesian grid through its endpoints. This is illustrated schematically in Fig. 2. At the wall it is anchored with a zero velocity boundary condition at the wall in each cut cell C. At the other end, there is a fixed point F (to use the same terminology as [4]) located a distance h_F from the boundary in the normal direction, which anchors it in the flow. (The use of a fixed distance away from the wall, instead of the cut cell centroid for example is needed to compensate for the wildly irregular cut cells in the mesh.) The solution at point F is obtained by interpolation from the Cartesian mesh. The velocity is then rotated into a normal and tangential frame of reference to obtain q_{tang}, the tangential velocity, using the normal vector defined by the portion of the boundary in cut cell C. A Newton iteration is used

[1] However Kalitzin et al. [9] have a nice approach that avoids iteration using pre-computed tables of inverses.

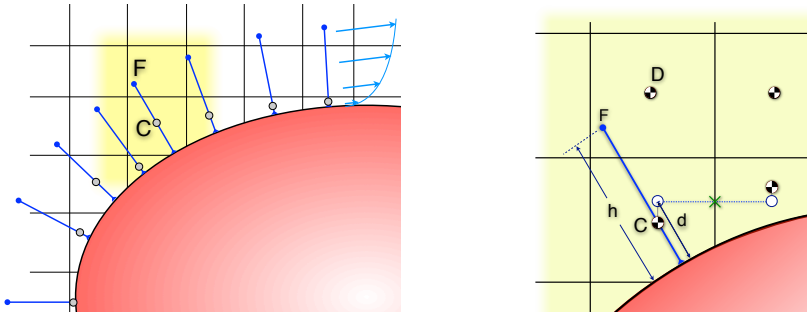

Figure 2: Illustration of construction for wall model coupling via constant height "forcing pts" through the centroids of the cut cells.

to find the friction velocity u_τ (see eq. (9)) so that the points lie on the wall function. Very few iterations are needed since the u_τ from the previous timestep provides a great starting guess for the next iteration.

Gradients of the model provide the viscous flux $\partial u/\partial y|_{y=0}$ needed at the wall by the finite volume scheme. The model also gives values of the tangential velocity needed to compute the difference at the cut faces (after rotating back to Cartesian velocity components u and v). Finally, we improve the gradient originally computed in a cut cell with the gradient of the solution to the wall model, evaluated at the cut cell centroid. (This was also done with the quadratic model for laminar flow). This provides a fully conservative coupling of the wall function and mesh, and makes maximal use of the wall function.

Figure 3 shows computational results from turbulent flow over a bump in a channel, taken from the NASA Langley Turbulence Modeling Resource [14] so we can compare with their results using CFL3D.

BVP Wall Models

There are several drawbacks to wall functions. For flows with separation, the skin friction, and u_τ, go to zero and the flow reverses. We will not be able to compute separation using a model in plus coordinates since that entails dividing by zero. Furthermore, the diffusion model assumes the convective terms are small, so cannot be used far from the wall where this is no longer true. It also assumes a mixing length model [10] for the turbulent viscosity, which is not true away from the wall after the initial linear growth.

We have developed a hierarchy of two point boundary value problems (bvp) that include increasingly more "physics", whose solution replaces the wall function. The first step was to actually replicate the wall function as a two point bvp. The diffusion model wall function (7) is already a bvp. By using the mixing length model for μ_t it can be easily solved and tested in our framework. We use the Shampine BVP solver for this, modified to run in parallel in a thread-safe way, save the solution between iterations,

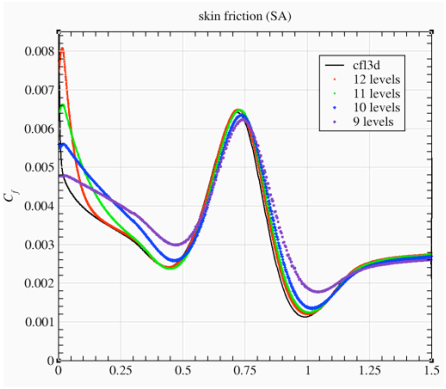

Figure 3: Skin friction using SA wall model on turbulent bump in channel problem. The wall model stays the same as the grid is refined. Without the wall model, many more mesh refinements are needed beyond our finest level grid.

etc. The solver takes a systems of first order equations, in this first case it is two equations, and $u(0)$ and $u(F)$ for the boundary conditions. As before, $u(F)$ is found by interpolation from the Cartesian grid. This eliminates the problem of $u_\tau \to 0$, since this works in physical coordinates and not plus coordinates. We then evaluate the solution $du/dy|_{y=0}$ to get u_τ, and compute the wall boundary conditions on the Cartesian side. The mixing length model we use is

$$\nu_t = \chi\nu = Ky^+\nu \qquad \text{and} \quad y^+ = yu_\tau Re_L/M_\infty, \tag{12}$$

so that the turbulent viscosity is proportional to the distance from the wall.

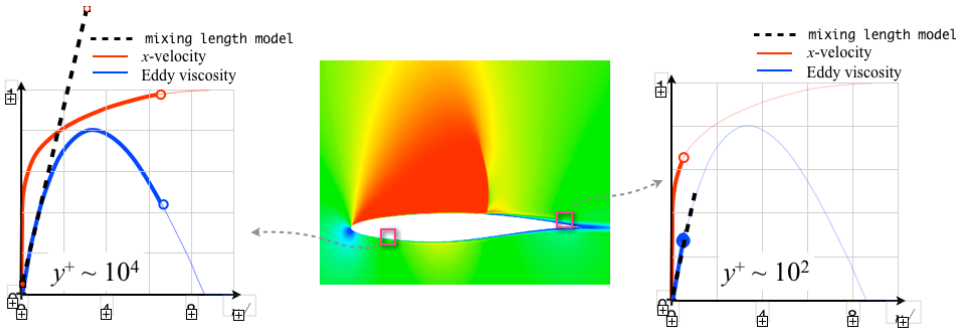

Figure 4: Results showing very different behavior of eddy viscosity profiles at different stations along wall, taken from very fine reference solution. AGARD case 10 RAE 2822 airfoil simulation [5].

However as Fig. 4 illustrates, this is only the first part of the turbulent viscosity computed by the RANS equations, valid only very close to the wall.

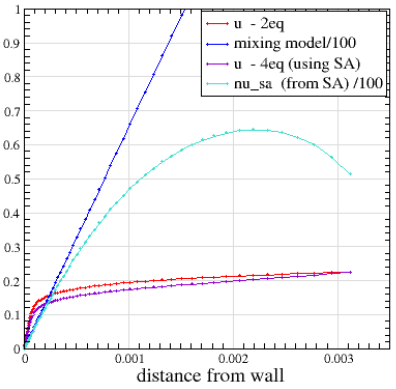

Figure 5: Results of solving the bvp using a mixing length model and an SA model for viscosity. The curvature in the eddy viscosity is well captured, and the tangnetial velocity changes somewhat as well.

The next step up in the hierarchy is to replace the mixing length model, and use as much of the Spalart-Allmaras turbulence model for ν_{sa} as is locally available. For example, all the normal derivatives that are already part of the bvp are included. We do not compute the terms involving streamwise derivatives.[2]. This gives the model

$$\frac{\partial}{\partial y}\left((\mu+\mu_t)\frac{\partial u}{\partial y}\right) = \frac{\partial p}{\partial x} \tag{13}$$

$$\frac{\partial}{\partial y}\left((\nu+\widetilde{\nu})\frac{\partial \widetilde{\nu}}{\partial y}\right) = \text{rest of diffusion terms} + \text{Prod} + \text{Dest} \tag{14}$$

When written as a system of first order equations this has dimension 4, and the new boundary conditions are $\nu_t(0) = 0$ at the wall, and $\nu_t(F)$, again specified via interpolation from the Cartesian grid. We initialize the solution using the previous iterate, or initially using the SA wall function and a mixing length model using the SA turbulence model. This helps the BVP solver converge quickly.

Using (most of) the SA turbulence equations allows much more variation in turbulent viscosity to be computed, see e.g. the profiles in the bottom row of Fig. 4. The streamwise velocity and especially the turbulent viscosity profiles vary greatly, depending on the location along the airfoil and the boundary layer thickness there. The four equation bvp model is able to compute the eddy viscosity even in this very nonlinear regime. Figure 5 shows a computation with our model compared to the mixing length model. The curvature in the eddy viscosity profile is captured very well.

We experimented for a long time with computing streamwise derivatives of terms in

[2]We use standard terminology and refer generically to the u velocity as the streamwise velocity, even though with cut cells it is more complicated, similarly for the v velocity, instead of saying normal and tangential velocities

these models, but found this to be too noisy to work. This involves differentiating from stations at the same normal location on each linelet. However the bvps are only solved to a tolerance, and differentiating them amplifies the noise. There is also noise coming from the changing location of point F relative to the Cartesian mesh, for example in the interpolation errors. Finally, there is the problem with the equation for the v velocity - the velocity in the normal direction. Asymptotically, this is really an equation for the pressure, and since it is orders of magnitude smaller than the streamwise velocity it is very hard to compute.

Instead, our highest fidelity model adds some convective terms taken from the background Cartesian grid to the equation for the tangential velocity. Those terms are zero at the wall, but as you go further into the boundary layer and approach the inviscid region, they are needed to balance the pressure gradient. We get the convective terms at point F again by interpolation from the Cartesian grid. However we have to be able to evaluate them at any point $y \in [0, F]$ to solve the bvp. For this we use a shut off function that goes from 0 at the wall, to 1 at point F. Altogether, our enhanced wall model together with the equation for the turbulent viscosity, is

$$\begin{aligned} \frac{\partial}{\partial y}\left((\mu+\mu_t)\frac{\partial u}{\partial y}\right) &= \frac{\partial p}{\partial x} + \psi(y)\left[u(F)\frac{\partial u(F)}{\partial x} + v(F)\frac{\partial u(F)}{\partial y}\right] \\ \frac{\partial}{\partial y}\left((\nu+\widetilde{\nu})\ \frac{\partial \widetilde{\nu}}{\partial y}\right) &= \text{rest of diffusion terms} + \text{Prod} + \text{Dest} \end{aligned} \tag{15}$$

Our model for ψ is

$$\psi(y) = SA(y)/SA(F),$$

which satisfies $\psi(0) = 0$ and $\psi(F) = 1$, where SA is the Spalart-Allmaras wall function.

We are submitting a paper with the details on this wall model to the AIAA in the coming month. Here we just show one result using this approach. We use an example of flow around a NACA 0012 from the Turbulence Modeling Resource website. There is a strong pressure gradient around the leading edge. Figure 6 shows skin friction for both the SA wall function and the bvp wall model. The SA wall function is not properly centered with respect to the converged CFL3D solution on either mesh, whereas the bvp model is aligned on even the coarser of the two mesh results. Other researchers have tried without success to include only a pressure gradient on the right-hand-side of the diffusion model [3]. We believe that is because the convective terms are of the same order as the pressure gradient, and all terms are needed to find the right balance. Note that the coarser of the two meshes in Fig. 6 has $y^+ \approx 500$ at the leading edge!

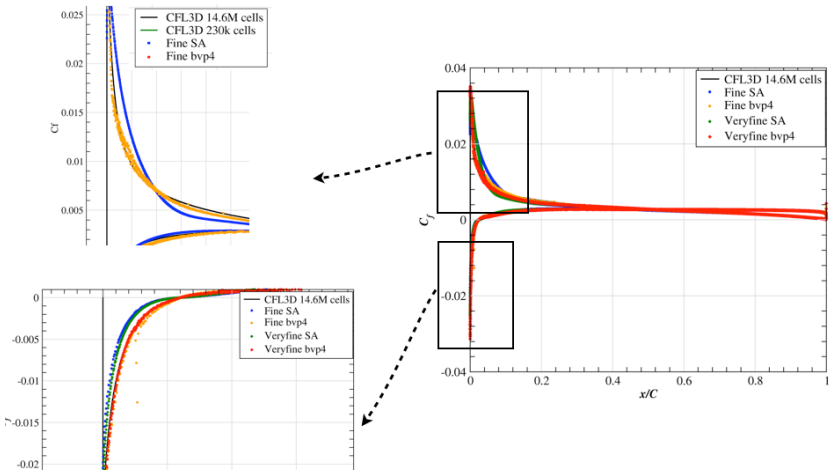

Figure 6: Comparison of SA wall function and bvp wall model for the NACA0012 case. This example convincingly shows how including the pressure gradient term centers the profile. The grid labeled 'Fine' (as opposed to Veryfine) has $y^+ \approx 500$ at the leading edge.

References

[1] S.R. Allmaras, F.T. Johnson, and P. R. Spalart. Modifications and clarifications for the implementation of the spalart-allmaras turbulence model. In *Seventh Intl. Conf. on Computational Fluid Dynamics (ICCFD7)*, July 2012. Big Island, HI.

[2] M. J. Berger and M. J. Aftosmis. Progress towards a Cartesian cut-cell method for viscous compressible flow, with an Appendix by Steve Allmaras. *AIAA-2012-1301*, Jan. 2012. Nashville, TN.

[3] R. B. Bond and Frederick G. Blottner. Derivation, implementation, and initial testing of a compressible wall-layer model. *Intl. J. Num. Methods Fluids*, 66:1183–1206, 2011.

[4] Francesco Capizzano. A turbulent wall model for immersed boundary methods. *AIAA-2010-712*, 2010.

[5] P. H. Cook, M. A. MacDonald, , and M. C. P. Firmin. Aerofoil RAE 2822 - Pressure Distributions, and Boundary-Layer and Wake Measurements. In *AGARD Advisory Report No. 138: Experimental Data Base for Computer Program Assessment*. North Atlantic Treaty Organization Advisory Group for Aerospace Research and Development, May 1979.

[6] T.J. Craft, S. E. Grant, H. Iacovides, and B. E. Launder. A new wall function strategy for complex turbulent flows. *Numerical Heat Transfer, Part B*, pages 301–318, 2004.

[7] A. Dadone. Towards a ghost cell method for analysis of viscous flows on cartesian grids. *AIAA-2010-709*, 2010.

[8] J.A. Fay and F.R. Riddell. Theory of stagnation point heat transfer in dissociated air. *J. Aeronaut. Sci.*, 25:73–85, 1958.

[9] G. Kalitzin, M. Goradz, G. Iaccarino, and P. Durbin. Near wall behavior of rans turbulence models and implications for wall functions. *J. Comp. Phys.*, 204:265–291, 2005.

[10] W. Kays, M. Crawford, and B. Weigand. *Convective Heat and Mass Transfer*. McGraw-Hill, 2005.

[11] Tobias Knopp, Thomas Alrutz, and Dieter Schwamborn. A grid and flow adaptive wall-function method for rans turbulence modelling. *J. Comp. Phys.*, 220:19–40, 2006.

[12] S. H. Myers and D. K. Walters. A one-dimensional subgrid near wall treatment for turbulent flow CFD simulation. In *Proceedings of IMECE 2005*, Paper IMCE 2005-81712, November 2005.

[13] P. Spalart and S. Allmaras. A one equation turbulence model for aerodynamic flows. *AIAA-92-0439*, 1992.

[14] Turbulence Modeling Resource Web Site. `http://turbmodels.larc.nasa.gov`.

1.

1. Report Type

Final Report

Primary Contact E-mail

Contact email if there is a problem with the report.

berger@cims.nyu.edu

Primary Contact Phone Number

Contact phone number if there is a problem with the report

2129983305

Organization / Institution name

Courant Institute, NYU

Grant/Contract Title

The full title of the funded effort.

High-Reynolds Number Viscous Flow on Embedded-Boundary Cartesian Grids

Grant/Contract Number

AFOSR assigned control number. It must begin with "FA9550" or "F49620" or "FA2386".

FA9550-13-1-0052

Principal Investigator Name

The full name of the principal investigator on the grant or contract.

Prof. Marsha Berger

Program Manager

The AFOSR Program Manager currently assigned to the award

Jean-Luc Cambier

Reporting Period Start Date

05/01/2013

Reporting Period End Date

04/30/2016

Abstract

Over the grant period, we developed a two-dimensional viscous steady- state flow solver for both laminar and turbulent flow. We developed a way to incorporate wall functions in non-body fitted grids by having each cut cell spawn a "linelet" from the wall through the cut cell centroid, into the Cartesian grid. We developed a fully conservative method for coupling the wall function to the flow on the Cartesian grid. We extended the wall function into a more general wall model that solves a two point boundary value problem on the linelets. The bvp includes more terms than is typically used in the diffusion model, which is what standard wall functions are based on. The improved wall model on the linelets allow them to go further into the boundary layer, reducing the Cartesian resolution requirements and allowing coarser near-wall Cartesian cells. This work was in collaboration with Michael Aftosmis, at NASA Ames Research Center.

Distribution Statement

This is block 12 on the SF298 form.

Distribution A - Approved for Public Release

Explanation for Distribution Statement

If this is not approved for public release, please provide a short explanation. E.g., contains proprietary information.

DISTRIBUTION A: Distribution approved for public release.

SF298 Form

Please attach your SF298 form. A blank SF298 can be found here. Please do not password protect or secure the PDF The maximum file size for an SF298 is 50MB.

SF298 .pdf

Upload the Report Document. File must be a PDF. Please do not password protect or secure the PDF . The maximum file size for the Report Document is 50MB.

finalReport.pdf

Upload a Report Document, if any. The maximum file size for the Report Document is 50MB.

Archival Publications (published) during reporting period:

"An Explicit Implicit scheme for Cut Cells in Embedded Boundary Meshes", with Sandra May. Submitted. Also SAM Research Report No. 2015-44, Dec. 2015.

"A note on the stability of cut cells and cell merging".
Appl. Num. Math. 96 (2015).

"A mixed explicit implicigt time stepping scheme for Cartesian embedded boundary meshes", with Sandra May. Proc. of Finite Volumes for Complex Applications VII, Springer, 2014.

Changes in research objectives (if any):

None

Change in AFOSR Program Manager, if any:

Previous AFOSR Program Manager was Fariba Fahroo.

Extensions granted or milestones slipped, if any:

None

AFOSR LRIR Number

LRIR Title

Reporting Period

Laboratory Task Manager

Program Officer

Research Objectives

Technical Summary

Funding Summary by Cost Category (by FY, $K)

	Starting FY	FY+1	FY+2
Salary			
Equipment/Facilities			
Supplies			
Total			

Report Document

Report Document - Text Analysis

Report Document - Text Analysis

Appendix Documents

2. Thank You

E-mail user